J Mol Model (2013) 19:4223–4237
DOI 10.1007/s00894-013-1880-2

ORIGINAL PAPER

DPT tautomerization of the long A·A* Watson-Crick base pair formed by the amino and imino tautomers of adenine: combined QM and QTAIM investigation

Ol'ha O. Brovarets' · Roman O. Zhurakivsky · Dmytro M. Hovorun

Received: 31 March 2013 / Accepted: 2 May 2013 / Published online: 29 May 2013

Abstract Combining quantum-mechanical (QM) calculations with quantum theory of atoms in molecules (QTAIM) and using the methodology of sweeps of the energetic, electron-topological, geometric and polar parameters, which describe the course of the tautomerization along the intrinsic reaction coordinate (IRC), we showed for the first time that the biologically important A·A* base pair (C_s symmetry) formed by the amino and imino tautomers of adenine (A) tautomerizes via asynchronous concerted double proton transfer (DPT) through a transition state (TS), which is the $A^+ \cdot A^-$ zwitterion with the separated charge, with C_s symmetry. The nine key points, which can be considered as electron-topological "fingerprints" of the asynchronous concerted A·A*↔A*·A tautomerization process via the DPT, were detected and completely investigated along the IRC of the A·A*↔A*·A tautomerization. Based on the sweeps of the H-bond energies, it was found that intermolecular antiparallel N6H···N6 (7.01 kcal mol^{-1}) and N1H···N1 (6.88 kcal mol^{-1}) H-bonds are significantly cooperative and mutually reinforce each other. It was shown for the first time that the A·A*↔A*·A tautomerization is assisted by the third C2H···HC2 dihydrogen bond (DHB), which, in contrast to the two others N6H···N6 and N1H···N1 H-bonds, exists within the IRC range from −2.92 to 2.92 Å. The DHB cooperatively strengthens, reaching its maximum energy 0.42 kcal mol^{-1} at IRC=−0.52 Å and minimum energy 0.25 kcal mol^{-1} at IRC =−2.92 Å, and is accompanied by strengthening of the two other aforementioned classical H-bonds. We established that the C2H···HC2 DHB completely satisfies the electron-topological criteria for H-bonding, in particular Bader's and all eight "two-molecule" Koch and Popelier's criteria. The positive value of the Grunenberg's compliance constant (5.203 Å/mdyn) at the $TS_{A\cdot A^*\leftrightarrow A^*\cdot A}$ proves that the C2H···HC2 DHB is a stabilizing interaction. NBO analysis predicts transfer of charge from σ(C2–H) bonding orbital to σ*(H–C2) anti-bonding orbital; at this point, the stabilization energy $E^{(2)}$ is equal to 0.19 kcal mol^{-1} at the $TS_{A\cdot A^*\leftrightarrow A^*\cdot A}$.

Keywords Amino and imino tautomers of adenine · Sweeps of the energetic, electron-topological, geometric and polar parameters along the IRC · The double proton transfer · Cooperativity of the H-bonds · CH···HC dihydrogen bond · B3LYP and MP2 levels of QM theory · QTAIM analysis

Electronic supplementary material The online version of this article (doi:10.1007/s00894-013-1880-2) contains supplementary material, which is available to authorized users.

O. O. Brovarets' · R. O. Zhurakivsky · D. M. Hovorun (✉)
Department of Molecular and Quantum Biophysics,
Institute of Molecular Biology and Genetics,
National Academy of Sciences of Ukraine, 150 Zabolotnoho Str,
03680 Kyiv, Ukraine
e-mail: dhovorun@imbg.org.ua

O. O. Brovarets' · R. O. Zhurakivsky · D. M. Hovorun
Research and Educational Center "State Key Laboratory of Molecular and Cell Biology", 150 Zabolotnoho Str,
03680 Kyiv, Ukraine

O. O. Brovarets' · D. M. Hovorun
Department of Molecular Biology, Biotechnology and Biophysics,
Institute of High Technologies, Taras Shevchenko National University of Kyiv, 2 Hlushkova Ave,
03127 Kyiv, Ukraine

Introduction

Adenine (A) occupies a prominent place among the canonical DNA bases [1]. It is believed that this nucleobase appeared first in the processes of abiogenic synthesis in the anoxic proto-atmosphere of the Earth [2, 3]. This observation is associated with the fact that, among all canonical

DNA bases and among all possible structural isomers of aminopurines with one and the same $C_5N_5H_5$ gross formula, only A is an energetically favorable isomer [4].

The complete family of molecular-zwitterionic prototropic tautomers of A comprises nine structures [5]. The most convincing biological role among these tautomers belongs to the A* imino form: it exactly mimics the guanine base and forms complementary bonds with cytosine base causing point mutations during DNA biosynthesis in the cell [6–8]. Experimental data on rare tautomers of the A base in the electronic ground state were absent in the literature until recently: information on them has been acquired only in a theoretical way [5, 7–12].

Recently, the long A·A* Watson-Crick base pair (Fig. 1), which is formed by the amino and imino tautomers of the A base joined by two antiparallel N1H···N1 and N6H···N6 hydrogen bonds (H-bonds), has been firmly established using X-ray analysis of the crystal structures of *Thermus thermophilus 30 S* [13–15] and *Haloarcula marismortui 50 S* ribosomal subunits [15, 16]. The authors of the work [15] considered the A·A* base pair as a static structure, in which imino and amino protons are localized in one of the two possible local minima: A·A* or A*·A.

The A base is also prone to deaminate spontaneously to hypoxanthine, generating, if left unrepaired, deleterious genomic mutation, namely A·T→G·C transitions, during DNA biosynthesis and resulting in genetic alterations potentially leading to cancer development or cell death [17–21]. In our recent works [22, 23] the molecular mechanisms of the mutation pressure exerted by hypoxanthine on DNA were thoroughly analyzed.

This work is aimed at understanding the structurally energetic and dynamic characteristics of the long A·A* Watson-Crick base pair, as well as its intrinsic properties. Using the sweeps (the result of the scanning of the changes of the certain physico-chemical characteristic along the IRC) of the energetic, electron-topological, geometric and polar parameters of the A·A*↔A*·A tautomerization via double proton transfer (DPT) along the intrinsic reaction coordinate (IRC), we established that it is a concerted (i.e., this reaction involves no stable intermediates) and asynchronous (i.e., protons move with a time gap) process. It should be noted that the tautomerization of the A·A* base pair (C_s) into the A*·A base pair (C_s) via the transition state (TS) (C_s), which is the $A^+{\cdot}A^-$ zwitterion with the separated charge, stabilized by the $N6^+H\cdots N6^-$ and $N1^+H\cdots N1^-$ H-bonds and the $C2^+H\cdots HC2^-$ dihydrogen bond (DHB), is none other than the tautomeric transition of the A·A* base pair into itself.

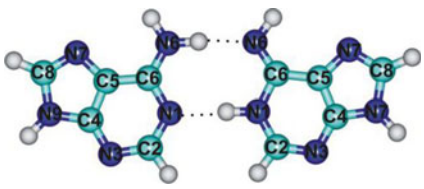

Fig. 1 Geometrical structure of the A·A* base pair (C_s). The numeration of atoms is generally accepted [78]. The intermolecular H-bonds are marked by *dashed lines*

Computational methods

All calculations were carried out with the Gaussian'09 suite of programs [24]. Geometries and harmonic vibrational frequencies of the A·A* and A*·A long base pairs and the TS of their tautomerization via the DPT were obtained using density functional theory (DFT) [25] with the B3LYP hybrid functional [26], which includes Becke's three-parameter exchange functional (B3) [27] combined with Lee, Yang and Parr's (LYP) correlation functional [28] in connection with Pople's 6-311++G(d,p) basis set in vacuum. A scaling factor of 0.9668 [7, 22, 23, 29–36] was used in the present work at the B3LYP quantum-mechanical (QM) level of theory to correct the harmonic frequencies of all the studied structures. We performed single point energy calculations at the correlated MP2 level of theory [37] with the 6-311++G(2df,pd) Pople's [38–40] and cc-pVTZ/cc-pVQZ Dunning's cc-type [41, 42] basis sets for B3LYP/6-311++G(d,p) geometries to consider electronic correlation effects as accurately as possible. MP2/6-311++G(2df,pd)//B3LYP/6-311++G(d,p), MP2/cc-pVTZ//B3LYP/6-311++G(d,p) and MP2/cc-pVQZ//B3LYP/6-311++G(d,p) levels of theory were applied successfully to similar systems, and have been verified to give accurate normal mode frequencies, barrier heights, characteristics of intra- and intermolecular H-bonds and geometries [3, 7, 22, 23, 29–36, 43–56]. Moreover, excellent agreement between computational and experimental NMR, UV and IR spectroscopic data [5, 35, 48, 50, 51] evidences that the levels of theory applied for the single-point energy calculations [MP2/6-311++G(2df,pd), MP2/cc-pVTZ and MP2/cc-pVQZ], as well as the method employed for the geometry optimisation [B3LYP/6-311++G(d,p)] are reliable.

The correspondence of the stationary points to local minima or TS on the potential energy landscape has been checked by the absence or the presence, respectively, of one and only one imaginary frequency corresponding to the normal mode that identifies the reaction coordinate. TS was located by means of the synchronous transit-guided quasi-Newton (STQN) method [57, 58].

Following location of the stationary points and TS, the reaction pathway was established by following the IRC in the forward and reverse directions from the TS using the Hessian-based predictor-corrector (HPC) integration algorithm [59–61] with tight convergence criteria. These calculations eventually ensure that the proper reaction pathway, connecting the expected reactants and products on each side of the TS, has been found. We investigated the evolution of the energetic,

geometric, polar and electron-topological characteristics of the H-bonds and base pairs along the reaction pathway, establishing them at each point of the IRC.

The electronic interaction energies, E_{int}, were computed at the MP2/6-311++G(2df,pd) level of theory for the geometries optimised at the DFT B3LYP/6-311++G(d,p) level of theory as the difference between the total energy of the base pair and the energies of the isolated monomers. In each case the interaction energy was corrected for the basis set superposition error (BSSE) [62, 63] through the counterpoise procedure [64, 65].

The Gibbs free energy G values for all structures were obtained at room temperature (T=298.15 K) in the following way:

$$G = E_{el} + E_{corr}, \quad (1)$$

where E_{el} is the electronic energy, and E_{corr} is the thermal correction.

The lifetime τ of the mispair can be estimated as $1/k_{f,r}$. The time $\tau_{99.9\ \%}$ necessary to reach 99.9 % of the equilibrium concentration of the A*·A reactant and the A·A* product of reaction in the system of reversible first-order forward (k_f) and reverse (k_r) reactions was estimated by the formula [66]:

$$\tau_{99.9\%} = \frac{ln10^3}{k_f + k_r}. \quad (2)$$

To estimate the values of the forward k_f and reverse k_r rate constants for the A·A*↔A*·A tautomerization reaction:

$$k_{f,r} = \Gamma \cdot \frac{k_B T}{h} e^{-\frac{\Delta\Delta G_{f,r}}{RT}} \quad (3)$$

we applied the standard TS theory [66], in which quantum tunneling effects are accounted by the Wigner's tunneling correction [67], that is adequate for the DPT reactions [3, 7, 22, 29–33, 36, 43]:

$$\Gamma = 1 + \frac{1}{24}\left(\frac{h\nu_i}{k_B T}\right)^2, \quad (4)$$

where k_B is the Boltzmann's constant, T=298.15 K is the temperature, h is Planck's constant, $\Delta\Delta G_{f,r}$ is Gibbs free energy of activation for the DPT reaction (T=298.15 K), R is the universal gas constant, and ν_i is the magnitude of the imaginary frequency associated with the vibrational mode at the TS that connects reactants and products.

Bader's quantum theory "atoms in molecules" (QTAIM) was applied to analyze electron density [68]. The topology of the electron density was examined using program package AIMAll [69] with all the default options. Wave functions were obtained at the level of theory used for geometry optimization. The presence of a bond critical point [68], namely the so-called (3,−1) bond critical point (BCP) and a bond path between hydrogen donor and acceptor, as well as the positive value of the Laplacian at this BCP ($\Delta\rho \geq 0$), were considered as three criteria for H-bond formation [68, 70]. Moreover, another five Koch and Popelier's criteria [70] dealing with changes in atomic properties (positive charge increase Δq, dipolar polarization decrease ΔM, reduction in atomic volume ΔV, energetic destabilization ΔE and mutual penetration of donor H_d and acceptor H_a hydrogen atoms [$\Delta r(H_d)+\Delta r(H_a)$] upon the formation of the hydrogen bond, were applied to test the $C2^{+}H\cdots HC2^{-}$ contact at the $TS_{A\cdot A^*\leftrightarrow A^*\cdot A}$ as DHB.

The energies of the conventional intermolecular H-bonds in the A·A* and A*·A base pairs and $TS_{A\cdot A^*\leftrightarrow A^*\cdot A}$ were evaluated by the empirical Iogansen's formula [71]:

$$E_{HB} = 0.33\cdot\sqrt{\Delta\nu - 40}, \quad (5)$$

where $\Delta\nu$ is the magnitude of the redshift (relative to the free molecule) of the stretching mode of the H-bonded groups involved in the H-bonding. The partial deuteration, namely the semi-deuteration of the amino group, was applied to eliminate the effect of vibrational resonances [3, 7, 22, 29–36, 43, 48–52].

The energies of all intermolecular H-bonds under the investigation of the sweeps of the H-bond energies were evaluated by the empirical Espinosa-Molins-Lecomte (EML) formula [72, 73] based on the electron density distribution at the (3,−1) BCPs of the H-bonds:

$$E_{HB} = 0.5\cdot V(r), \quad (6)$$

where V(r) is the value of a local potential energy at the (3,−1) BCPs.

Moreover, the relative strength of the C2H···HC2 DHB was estimated by means of Grunenberg's compliance constants formalism [74–76]. In contrast to force constants, the numerical values of compliance constants do not depend on the coordinate system. The physical meaning of compliance constants is deduced from their definition as partial second derivative of the potential energy due to an external force:

$$C_{ij} = \partial^2 E \Big/ \partial f_i \partial f_j. \quad (7)$$

In other words, compliance constants measure the displacement of an internal coordinate resulting from a unit force acting on it. As follows from this definition, a lower numerical value of compliance constant represents a stronger bond. The compliance constants were calculated using Compliance 3.0.2 program [74–76].

To study the charge transfer property in the interacting orbitals of the $C2^{+}H\cdots HC2^{-}$ DHB at the $TS_{A\cdot A^*\leftrightarrow A^*\cdot A}$, we resorted to natural bond orbital (NBO) analysis [77], which interprets the electronic wave function in terms of a set of occupied Lewis and a set of unoccupied non-Lewis localized orbitals. A second-order Fock matrix analysis was carried out

to evaluate interactions between donor (i) and acceptor (j) bonds. The result of such interaction is a migration of the electron density from the idealized Lewis structure into an empty non-Lewis orbital σ^*. For each donor (i) and acceptor (j) bond, the stabilization energy is:

$$E^{(2)} = \Delta E_{ij} = q_i \frac{F(i,j)^2}{\varepsilon_j - \varepsilon_i}, \quad (8)$$

where q_i is the donor orbital occupancy, ε_j and ε_i are diagonal elements and F(i,j) is the off diagonal element of NBO Fock matrix.

The atomic numbering scheme for the A nucleobase is conventional [78]. All distances including IRC are presented in the text in Å (1 Bohr=0.52918 Å).

Results and discussion

The obtained results are presented in Tables 1, 2, 3, and 4 and Figs. 2, 3, 4, 5, 6, 7, 8, and 9 and S1. Their analysis allows us to make the following conclusions.

We have shown for the first time that the A·A*↔A*·A tautomerization via the DPT is a concerted (i.e., the reaction involves no stable intermediates) and asynchronous process (i.e., the A·A* base pair sequentially converts to the A*·A base pair by the migration of the proton localized at the N1 nitrogen atom of the A* imino tautomer along the N1H···N1 H-bond to the N1 nitrogen atom of the A base and then through the TS, which is the $A^+ \cdot A^-$ zwitterion with the separated charge, the proton localized at the N6 nitrogen atom of the A^+ protonated base transitions to the N6 nitrogen atom of the A^- deprotonated base).

The equivalent from a symmetrical point of view A·A* and A*·A base pairs, which are biologically important and defined in the literature as long Watson-Crick base pairs [15], are planar structures with C_s symmetry, despite the fact that A, in common with other DNA bases, is a flexible molecule [56, 79, 80]. The A·A* and A*·A base pairs are stabilized by two antiparallel and energetically almost equivalent upper N6H···N6 (7.06 kcal mol^{-1}), exposed in the major groove of the double-stranded DNA, and the middle N1···HN1 (6.88 kcal mol^{-1}) H-bonds (Tables 1, 2). The $TS_{A\cdot A^*\leftrightarrow A^*\cdot A}$ with imaginary frequency ν_i=497.5*i* cm^{-1} also has C_s symmetry. Notably, the TS of the A·A*↔A*·A tautomerization is the ion pair $A^+ \cdot A^-$ stabilized by the two parallel and quite strong $N6^+H\cdots N6^-$ (13.92 kcal mol^{-1}) and $N1^+H\cdots N1^-$ (13.50 kcal mol^{-1}) conventional H-bonds and one weak $C2^+H\cdots HC2^-$ (0.42 kcal mol^{-1}) DHB (Tables 1, 2).

It is interesting to note that the total energy ΣE_{HB} of the N6H···N6 and N1···HN1 H-bonds in the A·A* or A*·A base pairs is notably less ($\Sigma E_{HB}/|\Delta E_{int}|$=77.6 %), than the electronic energy of the interaction of the A and A* bases in the pair (ΔE_{int}=−17.89 kcal mol^{-1}). The energy relationship $\Sigma E_{HB}/|\Delta E_{int}|$ cannot be considered as the physico-chemical characteristic exceptionally of the A·A* and A*·A base pairs and was used for the characterization of the other H-bonded base pairs [3, 7, 22, 43]. The A·A* and A*·A base pairs are thermodynamically stable structures with ΔG_{int}=−4.32 kcal mol^{-1} at room temperature. It was established that the A·A* and A*·A base pairs are dynamically stable structures [43, 56, 81], as their zero-point energy (1,560.2 cm^{-1}) of the corresponding vibrational mode, which frequency becomes imaginary at the TS of the A·A*↔A*·A tautomerization, is less than the value of the reverse barrier $\Delta\Delta E_{TS}$=10.33 kcal mol^{-1} or 3,612.8 cm^{-1} obtained at the MP2/cc-pVQZ//B3LYP/6-311++G(d,p) level of QM theory (Table 3).

Establishing the several types of properties, namely, the electronic energy, the first derivative of the electronic energy with respect to the IRC, the dipole moment of the A·A* base pair, the intermolecular H-bond distances, the electron density, the Laplacian of the electron density, the energy at the BCPs of the intrapair H-bonds and the distance between the glycosidic protons at each step along the IRC of the A·A*↔A*·A tautomerization, we obtained the sweeps of these characteristics presented in Figs. 2, 3, 4, 5, 6, 7, 8, and 9 and S1.

We revealed nine key points for A·A*↔A*·A tautomerization (Fig. 2) similar to those obtained previously in our recent studies [3, 23]; three of these key points represent stationary structures—the $TS_{A\cdot A^*\leftrightarrow A^*\cdot A}$ (key point 5), the initial state (the A·A* reactant; key point 1) and the final state, i.e., the A*·A product (key point 9), which is equivalent to the reactant. The other six key points are predefined by the structural and electronic rearrangements of the A·A* base pair along the IRC.

Key point 1. The starting structure along the IRC pathway is the A·A* base pair with Watson-Crick geometry. It is stabilized by the N6H···N6 and N1···HN1 cooperative H-bonds (Tables 1, 2; Figs. 2, 6c).

Key point 2. The structure of the base pair, for which the H–N1 chemical bond of the A* base is significantly weakened and the N1···H H-bond actually becomes the N1–H covalent bond ($\Delta\rho_{N1\cdots H}$=0) (Figs. 2, 6b). The maximum value of the energy of the N1···H H-bond is reached at this key point (Fig. 6c). Interestingly, one of the two extrema of the first derivative of the electron energy with respect to the IRC dE/dIRC (well known in the literature as reaction force [82–87]) is reached exactly at this key point (Fig. 3a, b). Moreover, precisely at key point 2, the A and A* bases, acting in this case as the reactants of the DPT reaction, lose their chemical individuality since the N1···H H-bond begins to transform into the N1–H covalent bond.

Table 1 Electron-topological, structural, vibrational and energetic characteristics of the intermolecular H-bonds in the A·A*, A*·A and $TS_{A\cdot A^*\leftrightarrow A^*\cdot A}$ obtained at the B3LYP/6-311++G(d,p) level of theory in vacuum. *IRC* Intrinsic reaction coordinate, *TS* transition state

Complex	AH···B H-bond	ρ[a]	$\Delta\rho$[b]	$100\cdot\varepsilon$[c]	$d_{A\cdots B}$[d]	$d_{H\cdots B}$[e]	Δd_{AH}[f]	∠AH···B[g]	$\Delta\nu$[h]	E_{HB}[i]
A·A* (IRC=−3.05 Å)	N6H···N6	0.035	0.091	7.19	2.918	1.885	0.028	176.3	491.5	7.01
	N1···HN1	0.034	0.087	6.76	2.943	1.904	0.030	179.0	474.6	6.88
$TS_{A\cdot A^*\leftrightarrow A^*\cdot A}$ (IRC=0.00 Å)	$N6^+H\cdots N6^-$	0.099	0.034	5.16	2.614	1.464	0.142	176.0	1,820.2	13.92
	$N1^+H\cdots N1^-$	0.098	0.029	4.70	2.637	1.479	0.144	179.5	1713.1	13.50
	$C2^+H\cdots HC2^-$	0.003	0.009	60.46	3.467	2.702	0.001	127.2	22.6	0.42*
A*·A (IRC=3.05 Å)	N6···HN6	0.035	0.091	7.19	2.918	1.885	0.028	176.3	491.5	7.01
	N1H···N1	0.034	0.087	6.76	2.943	1.904	0.030	179.0	474.6	6.88

[a] Electron density at the bond critical point (BCP), a.u.

[b] Laplacian of the electron density at the BCP, a.u.

[c] Ellipticity at the BCP

[d] Distance between A (H-bond donor) and B (H-bond acceptor) atoms, Å

[e] Distance between H and B atoms, Å

[f] Elongation of the H-bond donating group AH upon H-bonding, Å

[g] H-bond angle, degree

[h] Redshift of the stretching vibrational mode of the AH H-bonded group, cm^{-1}

[i] H-bond energy, estimated by Iogansen's [70] or Espinose-Molins-Lecomte (EML) formulae (marked with an asterisk) [71, 72], kcal mol^{-1}

Table 2 Electron-topological, structural and energetic characteristics of the intermolecular H-bonds revealed in the structures of the nine key points obtained at the B3LYP/6-311++G(d,p) level of theory in vacuum. For footnote definitions, see Table 1

Complex	AH···B H-bond	ρ	$\Delta\rho$	$100\cdot\varepsilon$	$d_{A\cdots B}$	$d_{H\cdots B}$	∠AH···B	E_{HB}
Key point 1 (A·A*) (IRC=−3.05 Å)	N6H···N6	0.035	0.091	7.19	2.918	1.885	176.3	7.01
	N1···HN1	0.034	0.087	6.76	2.943	1.904	179.0	6.88
Key point 2 ($\Delta\rho_{N1\cdots H}$=0, IRC=−0.31 Å)	N6H···N6	0.078	0.093	5.58	2.635	1.553	175.3	25.16*
	N1···HN1	0.112	0.000	4.18	2.621	1.418	180.0	37.45*
	C2H···HC2	0.003	0.009	48.67	3.459	2.700	126.6	0.42*
Key point 3 ($\rho_{N1H}=\rho_{HN1}$, IRC=−0.19 Å)	N6H···N6	0.083	0.080	5.50	2.631	1.532	175.4	26.68*
	N1-H-N1	0.148	−0.196	5.10	2.622	1.311	179.7	-
	C2H···HC2	0.003	0.009	53.06	3.461	2.700	126.8	0.42*
Key point 4 ($\Delta\rho_{H\cdots N1}$=0, IRC=−0.05 Å)	N6H···N6	0.092	0.054	5.31	2.621	1.131	175.7	29.75*
	N1H···N1	0.107	0.000	4.49	2.631	1.187	179.5	34.53*
	C2H···HC2	0.003	0.009	58.77	3.465	2.701	127.1	0.42*
Key point 5 ($TS_{A\cdot A^*\leftrightarrow A^*\cdot A}$) (IRC=0.00 Å)	$N6^+H\cdots N6^-$	0.099	0.034	5.16	2.614	1.464	176.0	13.92
	$N1^+H\cdots N1^-$	0.098	0.029	4.70	2.637	1.479	179.5	13.50
	$C2^+H\cdots HC2^-$	0.003	0.009	60.46	3.467	2.702	127.2	0.42*
Key point 6 ($\Delta\rho_{H\cdots N6}$=0, IRC=0.05 Å)	N6H···N6	0.109	0.000	4.94	2.606	1.426	176.2	35.90*
	N1H···N1	0.092	0.047	4.86	2.642	1.503	179.5	29.27*
	C2H···HC2	0.003	0.009	61.21	3.469	2.703	127.3	0.42*
Key point 7 ($\rho_{N6H}=\rho_{HN6}$, IRC=0.19 Å)	N6-H-N6	0.150	−0.200	4.01	2.596	1.298	176.6	–
	N1H···N1	0.083	0.073	5.08	2.649	1.540	179.5	26.54*
	C2H···HC2	0.002	0.009	59.91	3.470	2.705	127.3	0.41*
Key point 8 ($\Delta\rho_{N6\cdots H}$=0, IRC=0.31 Å)	N6···HN6	0.113	0.000	4.53	2.593	1.409	176.8	38.76*
	N1H···N1	0.079	0.086	5.20	2.652	1.561	179.5	25.15*
	C2H···HC2	0.002	0.009	57.92	3.471	2.705	127.3	0.41*
Key point 9 (A*·A) (IRC=3.05 Å)	N6···HN6	0.035	0.091	7.19	2.918	1.885	176.3	7.01
	N1H···N1	0.034	0.087	6.76	2.943	1.904	179.0	6.88

Table 3 Energetic and kinetic characteristics of the A·A*↔A*·A tautomerization via double proton transfer (DPT) in vacuo obtained at the different levels of quantum-mechanical (QM) theory

Level of QM theory	$\Delta\Delta G_{TS}$[a]	$\Delta\Delta E_{TS}$[b]		ν[c]	E_{ZPE}[d]	τ[e]	$\tau_{99.9\ \%}$[f]
		kcal mol^{-1}	cm^{-1}				
MP2/6-311++G(2df,pd)//B3LYP/6-311++G(d,p)	6.51	9.83	3,438.9	3,120.4	1,560.2	$7.87\cdot10^{-9}$	$2.72\cdot10^{-8}$
MP2/cc-pVTZ//B3LYP/6-311++G(d,p)	6.99	10.31	3,604.9	3,120.4	1,560.2	$1.75\cdot10^{-8}$	$6.06\cdot10^{-8}$
MP2/cc-pVQZ//B3LYP/6-311++G(d,p)	7.01	10.33	3,612.8	3,120.4	1,560.2	$1.82\cdot10^{-8}$	$6.29\cdot10^{-8}$

[a] Gibbs free energy of activation for the forward and reverse reactions of tautomerization (T=298.15 K), kcal mol^{-1}

[b] Activation electronic energy for the forward and reverse reactions of tautomerization

[c] Frequency of the vibrational mode of the tautomerized complex which becomes imaginary in the TS of tautomerization, obtained at the B3LYP/6-311++G(d,p) level of geometry optimization (cm^{-1})

[d] Zero-point vibrational energy associated with this normal mode (cm^{-1})

[e] Lifetime of the A·A*/A*·A base pair (s)

[f] Time necessary to reach 99.9 % of the equilibrium concentration of the reagent A·A* and the product A*·A of the A·A*↔A*·A tautomerization reaction via the DPT (s)

Key point 3. The structure is characterized by the equivalent loosened N1–H and H–N1 covalent bonds. Dependencies of the geometrical and electron-topological characteristics at the BCPs of these equivalent chemical bonds intersect exactly at this key point, forming χ-like graphs for the loosened N1–H–N1 bridge ($\rho_{N1\text{-}H}=\rho_{H\text{-}N1}=0.148$ a.u.; $\Delta\rho_{N1\text{-}H}=\Delta\rho_{H\text{-}N1}=-0.196$ a.u.; $d_{N1\text{-}H}=d_{H\text{-}N1}=1.311$ Å; $d_{N1\cdots N1}=2.622$ Å; ∠N1–H–N1=179.7°) (Table 2, Figs. 2; 6a, b; 7).

Key point 4. At this structure situated quite close to the $TS_{A\cdot A^*\leftrightarrow A^*\cdot A}$ the H–N1 covalent bond becomes the H···N1 H-bond (Fig. 2). A characteristic feature of this structure is a zero value of the Δρ at the BCP of the H···N1 H-bond (Fig. 6b). The maximum value of the energy of the H···N1 H-bond is attained at this key point (Fig. 6c).

Key point 5. The $TS_{A\cdot A^*\leftrightarrow A^*\cdot A}$ of the tautomerization via the DPT, which itself represents an ion pair $A^+\cdot A^-$, is stabilized by the $N6^+H\cdots N6^-$ and $N1^+H\cdots N1^-$ canonical H-bonds and the $C2^+H\cdots HC2^-$ DHB (Tables 1, 2; Figs. 2, 6c).

Key point 6. The structure of the base pair, for which the N6–H chemical bond of the A^+ base is significantly weakened and the H···N6 H-bond actually becomes the H–N6 covalent bond ($\Delta\rho_{H\cdots N6}=0$) (Figs. 2, 6b). The maximum value of the energy of the H···N6 H-bond is reached at this key point (Fig. 6c).

Key point 7. This structure possesses the equivalent loosened N6-H and H-N6 covalent bonds. Dependencies of the geometrical and electron-topological characteristics at the BCPs of these equivalent chemical bonds intersect exactly at this key point, forming χ-like graphs for the loosened N6-H-N6 bridge ($\rho_{N6\text{-}H}=\rho_{H\text{-}N6}=0.150$ a.u.; $\Delta\rho_{N6\text{-}H}=\Delta\rho_{H\text{-}N6}=-0.200$ a.u.; $d_{N6\text{-}H}=d_{H\text{-}N6}=1.298$ Å; $d_{N6\cdots N6}=2.596$ Å; ∠N6-H-N6=176.6°) (Table 2, Figs. 2; 6a, b;).

Table 4 Change of atomic properties of the donor H_d and acceptor H_a hydrogen atoms involved in the intermolecular $C2^+H\cdots HC2^-$ dihydrogen bond (DHB) in the $TS_{A\cdot A^*\rightarrow A^*\cdot A}$ obtained at the B3LYP/6-311++G(d,p) level of theory in vacuum. $\Delta r(H_d)+\Delta r(H_a)$ − mutual penetration, i.e., the sum of the variations of atomic radii of donor H_d and acceptor H_a hydrogen atoms upon the formation of the $C2^+H\cdots HC2^-$ DHB. All changes of values are indicated with respect to free monomers (bases)

$q(H_d)$[a]	Δq	$M(H_d)$[b]	$-\Delta M$	$V(H_d)$[c]	$-\Delta V$	$-E(H_d)$[d]	ΔE	$r(H_d)$[e]	$r(H_a)$[f]	$\Delta r(H_d)$[g]	$\Delta r(H_a)$[h]
0.928	0.021	0.129	0.007	47.1	0.3	0.599	0.009	2.51	2.59	0.02	0.03

[a] Atomic charge (a.u.)

[b] Dipolar polarization (a.u.)

[c] Atomic volume (a.u.)

[d] Energy of the atom (a.u.)

[e] Radius of the donor H_d hydrogen atom upon the formation of the $C2^+H\cdots HC2^-$ DHB (a.u.)

[f] Radius of the acceptor H_a hydrogen atom upon the formation of the $C2^+H\cdots HC2^-$ DHB (a.u.)

[g] Variation of atomic radius of donor H_d hydrogen atom upon the formation of the $C2^+H\cdots HC2^-$ DHB (a.u.)

[h] Variation of atomic radius of acceptor H_a hydrogen atom upon the formation of the $C2^+H\cdots HC2^-$ DHB (a.u.)

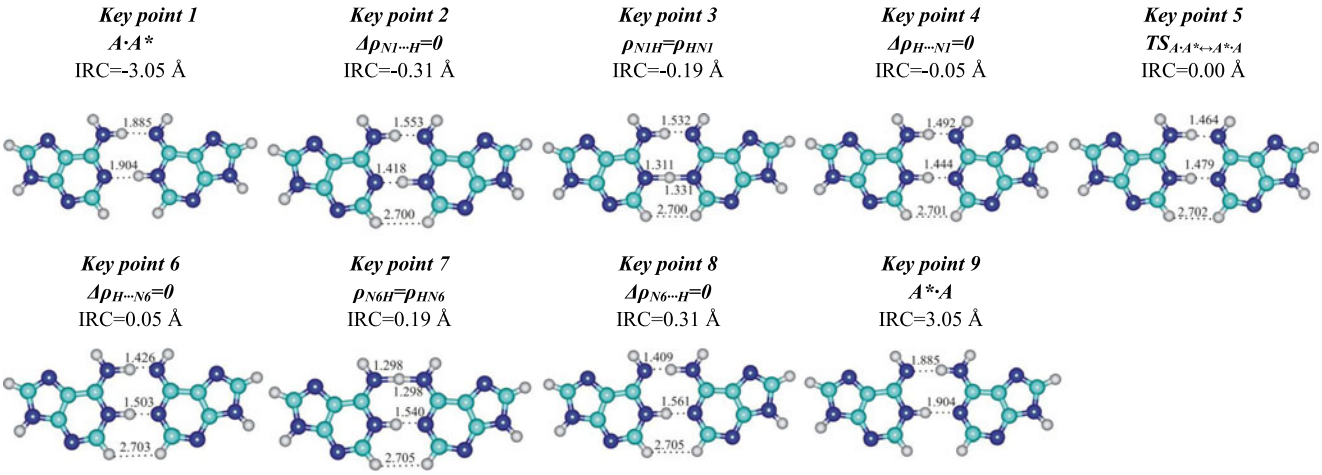

Fig. 2 Geometric structures of the nine key points describing the evolution of the A·A*↔A*·A tautomerization via the double proton transfer (DPT) along the intrinsic reaction coordinate (IRC) obtained at the B3LYP/6-311++G(d,p) level of theory in vacuo. The coordinates of each key point are presented above it. The *dotted lines* indicate AH···B H-bonds and C2H···HC2 dihydrogen bond (DHB), while continuous lines show covalent bonds (lengths in Ångstroms). Atoms: *light-blue* carbon, *dark-blue* nitrogen, *grey* hydrogen

Key point 8. At this structure, which is situated quite close to the final A*·A base pair and in which the mispair containing amino and imino tautomers of the A base begins to form, the N6–H covalent bond becomes the N6···H H-bond (Fig. 2). A characteristic feature of this structure is a zero value of the Δρ at the BCP of the H···N6 H-bond (Fig. 6b). The maximum value of the energy of the N6···H H-bond is attained at this key point (Fig. 6c). Interestingly, the second extremum of the first derivative of the electron energy with respect to the IRC dE/dIRC (well known in the literature as reaction force constant [82–87]) is reached exactly at this key point (Fig. 3a,b). It should be noted that, precisely at the key point 8, the A and A* bases, acting in this case as the products of the DPT reaction, reduce their chemical individuality, since the N6–H covalent bond begins to transform into the N6···H H-bond.

Key point 9. The final structure is the tautomerized A*·A base pair, stabilized by the N6···HN6 and N1H···N1 cooperative H-bonds (Tables 1, 2; Figs. 2, 6c).

These nine key points [3, 23] are used to define the reactant, TS and product regions of the A·A*↔A*·A tautomerization via the DPT (Figs. 2, 3b). The division of the reaction pathway into the reaction, TS and product region can be done quite naturally and unambiguously by taking the reaction force minimum and the reaction force maximum as the boundaries for these regions [82–87]. So,

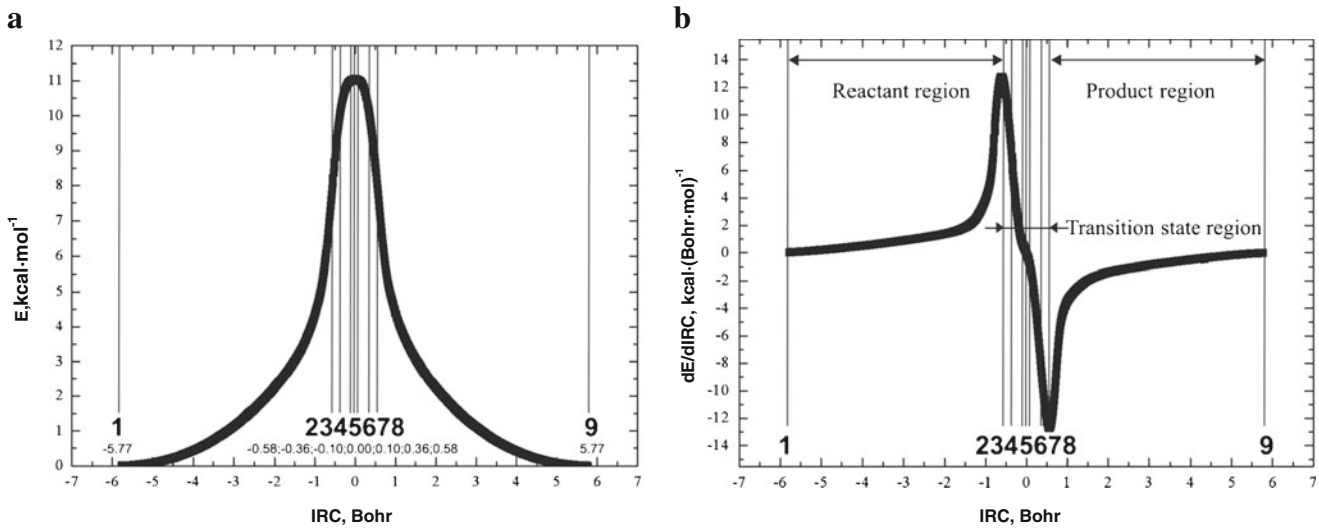

Fig. 3 Profiles of **a** the electronic energy E, and **b** the first derivative of the electronic energy with respect to the IRC dE/dIRC along the IRC of the A·A*↔A*·A tautomerization via the DPT obtained at the B3LYP/6-311++G(d,p) level of theory in vacuo

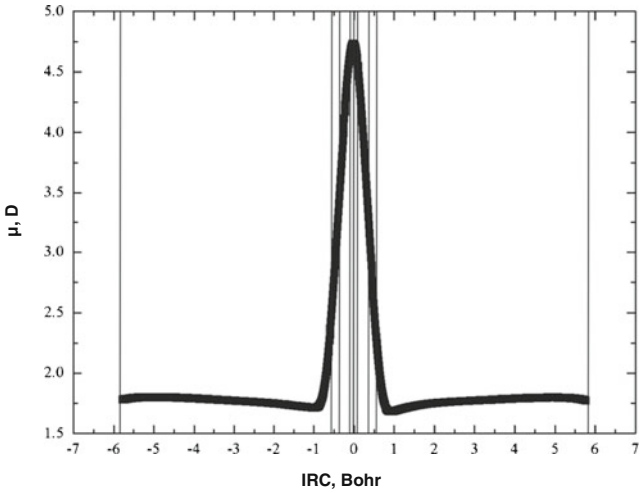

Fig. 4 Profile of the dipole moment μ along the IRC of the A·A*↔A*·A tautomerization via the DPT obtained at the B3LYP/6-311++G(d,p) level of theory in vacuo

nucleotide bases do not lose their chemical individuality at the reactant and product regions, which are located between the key points 1–2 and 8–9, respectively, and acquire the mutual deformation and orientation that eventually lead to the chemical reaction at the TS region, namely to the DPT. It follows quite logically from the obtained by us sweeps of the Δρ that the reactant region starts at key point 1 and ends at key point 2. The product region, where the rare tautomers of nucleotide bases do not lose their chemical individuality and where the relaxation to the final A*·A base pair takes place, begins at key point 8 and ends at the final key point 9. Actually, the TS region, where the DPT occurs, is located between key points 2 and 8. At the reactant region, the A·A* base pair rearranges in order to run the DPT chemical reaction. We established that the electronic energy necessary to bring the donor and acceptor atoms as close as possible to each other to activate the DPT reaction, i.e., the energy difference between key points 2 and 1, is 7.74 kcal mol^{-1}, representing 70.1 % of the TS energy. An equivalent quantity of energy is released at the relaxation of the base pair, corresponding to key point 8, under its tautomerization into the reaction product: the A*·A base pair. A characteristic feature of the A·A*↔A*·A tautomerization is the rather narrow zone of the essentially DPT chemical reaction, which lies within the IRC range from −0.31 to 0.31 Å (Fig. 3b).

We established that the A·A* base pair "breathes" throughout the tautomerization process, thereby maintaining its Watson-Crick geometry (Figs. 7a,b; 9). The compression of the starting A·A* or the final A*·A base pairs at the TS region, especially at the $TS_{A\cdot A^*\leftrightarrow A^*\cdot A}$, occurs due to the contraction of the distances between the N6 (by 0.306 Å) and N1 nitrogen atoms (by 0.292 Å) and the C2 carbon atoms (by 0.268 Å) (Figs. 7a,b; 9). This phenomenon is also represented by the changes of α_1 and α_2 glycosidic angles (by 1.3°) and R(H–H) distance between the glycosidic protons (by 0.272 Å) (Fig. 9). Moreover, the R(H–H) distance does not depend on IRC and remains almost constant (12.03 Å) (Fig. 9) within the IRC range from −0.72 to 0.72 Å. Changes in the R(H–H) distance are accompanied by the distortion of the glycosidic angles α that leads to their oscillations within the range 45.9–47.2°. The ∠N1HN1 angle insignificantly changes (178.5–180.0°), while the ∠N6HN6 angle varies strongly (173.7–177.1°) along the IRC. Ellipticity of the classical intermolecular N6H···N6 and N1H···N1 H-bonds non-monotonically varies within the range from 0.031 to 0.072 along the IRC (Fig. S1).

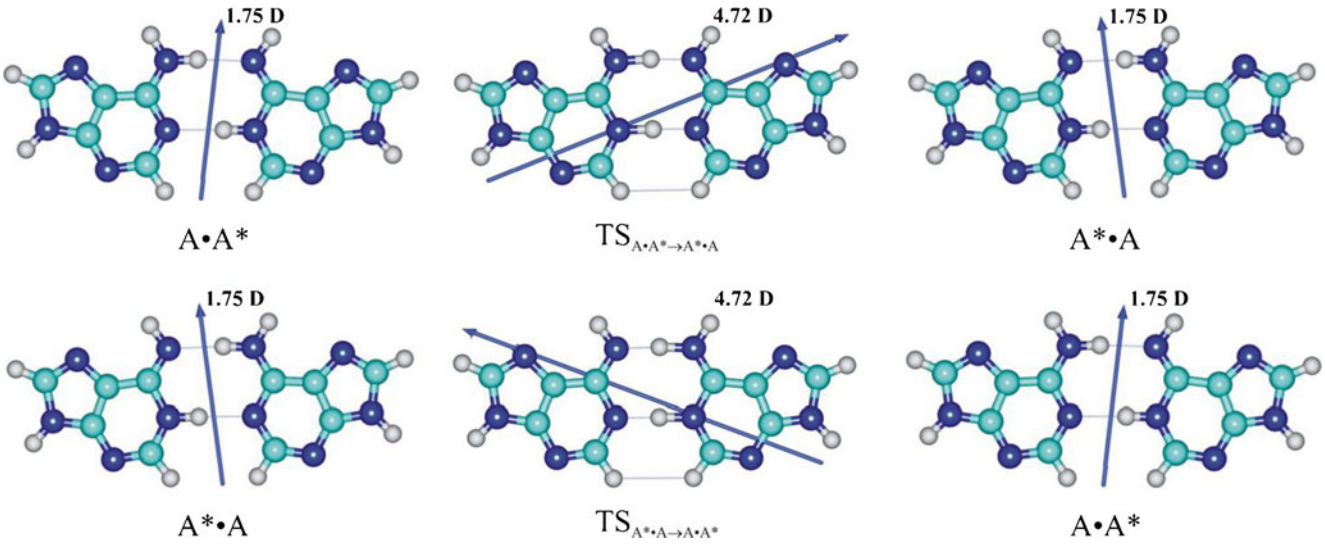

Fig. 5 Change in magnitude and orientation of the dipole moment vector at the A·A*↔A*·A (*upper row*) and A*·A↔A·A* (*lower row*) tautomerizations through the DPT obtained at the B3LYP/6-311++G(d,p) level of theory in vacuo. The structures corresponding to the stationary points and their dipole moments are presented

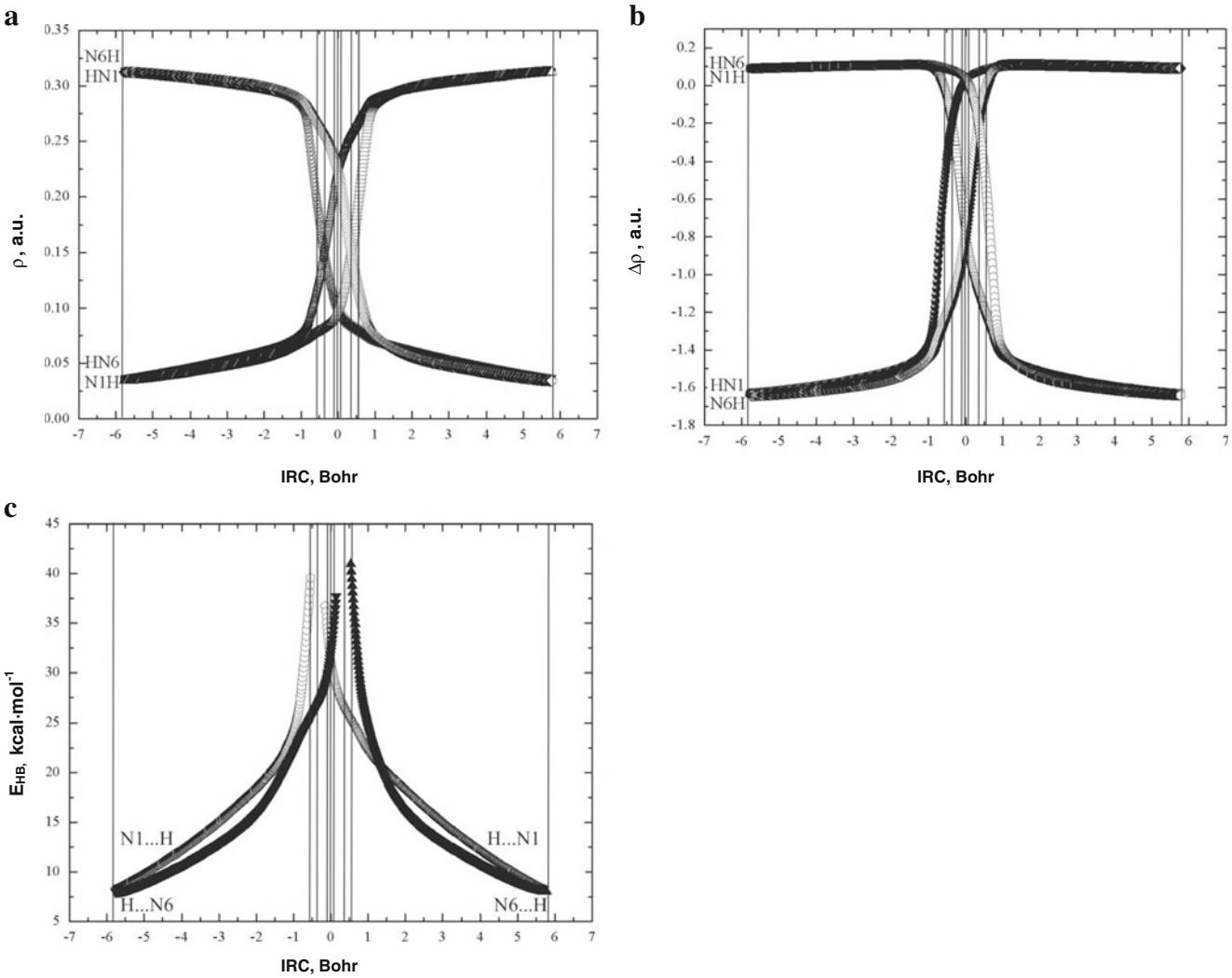

Fig. 6 Profiles of **a** the electron density ρ, **b** the Laplacian of the electron density Δρ, and **c** the energy of the H-bond E_{HB}, estimated by the EML formula [72, 73], at the BCPs of the covalent and hydrogen bonds along the IRC of the A·A*↔A*·A tautomerization via the DPT obtained at the B3LYP/6-311++G(d,p) level of theory in vacuo

The strong dependence of both the absolute value and the orientation of the dipole moment of the studied base pairs in the DPT process on the IRC has been revealed (Figs. 4, 5). Thus, we came to the conclusion that the investigated A·A* base pair cannot be considered as a static structure, since it performs dipole-active movements with large amplitude through the DPT, transforming to the A*·A symmetric state and vice versa.

The upper N6H···N6 and the middle N1···HN1 H-bonds in the A·A* base pair exist within the 1–6 and 1–2 structures, respectively, becoming coherently stronger during the tautomerization process, while the upper N6···HN6 and the middle N1H···N1 H-bonds in the A*·A base pair exist within the 8–9 and 4–9 structures, respectively, becoming coherently weaker during the tautomerization process in vacuum (Fig. 6c). It should be noted that the graphs show the energy of only those H-bonds corresponding to the value Δρ≥0 (Fig. 6b).

Analysis of the dependencies of the H-bond energies on the IRC listed in Fig. 6c allows us to make a definite conclusion that they are significantly cooperative [3, 22, 91] ($dE_{N1\cdots HN1}/dE_{N6H\cdots N6}$=11.90/1.00) and mutually reinforce each other.

We established that the A·A*↔A*·A tautomerization is assisted by the third C2H···HC2 DHB [48–53, 88, 89], which, in contrast to the two others H-bonds, exists within the IRC range from −2.92 to 2.92 Å (Fig. 8). The C2H···HC2 DHB cooperatively strengthens, reaching its maximum energy 0.42 kcal mol^{-1} at IRC=−0.52 Å and minimum energy 0.25 kcal mol^{-1} at IRC=−2.92 Å, and is accompanied by strengthening of the two aforementioned classical H-bonds. To distinguish between H-bond donating (donor) and accepting (acceptor) C2H groups, we compared NBO charges on the hydrogen atoms of these groups [48–53, 92, 93]. It was found that the hydrogen atom of the C2H group in the A^+ base bears a

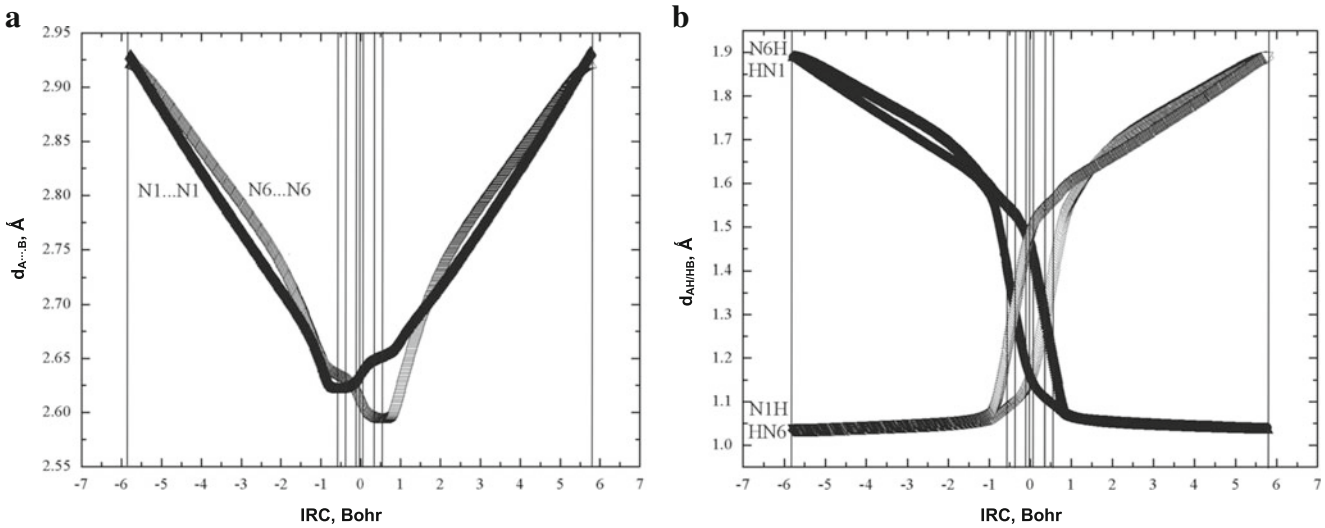

Fig. 7 Profiles of **a** the distance $d_{A\cdots B}$ between the electronegative A and B atoms, and **b** the distance $d_{AH/HB}$ between the hydrogen and electronegative A or B atoms of the AH···B H-bonds along the IRC of the A·A*↔A*·A tautomerization via the DPT obtained at the B3LYP/6-311++G(d,p) level of theory in vacuo

greater positive charge (0.188 e) than the corresponding hydrogen in the A^- base (0.160 e) at the $TS_{A\cdot A^*\leftrightarrow A^*\cdot A}$, and thus can be considered as the H-bonding donor, while the hydrogen atom of the C2H group in the A^- base serves as the acceptor (Fig. 8f).

The $C2^+H(A^+)\cdots HC2^-(A^-)$ interaction at the $TS_{A\cdot A^*\rightarrow A^*\cdot A}$ does not meet the geometric requirements for the H-bonding determined by Bondi [94], since the distance between the donor and acceptor groups exceeds the double Bondi's van der Waals radius of the hydrogen atom: d_{HH}(2.70 Å)> $2r_H^{vdW}$(2.40 Å). However, a van der Waals cutoff is not the physical limit of the long-range electrostatic H-bond interaction [95] and can act beyond this distance [96]. Moreover, the hydrogen bond radii for CH group have been recently revised in the literature and established to be 1.10±0.20 Å; it appears that a CH group could have a radius larger than 1.2 Å when involved in H-bonding [97].

The $C2^+H\cdots HC2^-$ DHB angle for the $TS_{A\cdot A^*\leftrightarrow A^*\cdot A}$ was established to be 127.2° (Tables 1, 2).

An extremely interesting situation was observed for the sweeps of the charges of the hydrogen atoms localized at the C2 carbon atoms along the IRC of the A·A*↔A*·A tautomerization via the DPT (Fig. 8f). The hydrogen atom localized at the C2 carbon atom in the amino form of A serves as the acceptor of the C2H···HC2 DHB, and the hydrogen atom localized at the C2 carbon atom in the imino form of A serves as the donor of the C2H···HC2 DHB within the IRC range from −2.92 to −0.31 Å, while the hydrogen atom localized at the C2 carbon atom in the amino form of A acts as the donor of the C2H···HC2 DHB and the hydrogen atom localized at the C2 carbon atom in the imino form of A serves as the acceptor of the C2H···HC2 DHB within the IRC range from −0.31 to 2.92 Å. Thus, the donor and acceptor hydrogen atoms interchange at key point 2 (IRC=−0.31 Å). The largest difference between the NBO charges of the donor and acceptor hydrogen atoms (0.028 e) is observed nearby the TS at IRC=0.04 Å. Moreover, based on these sweeps of NBO charges (Fig. 8f) it can be asserted that, strictly speaking, the C2H···HC2 DHB can be considered as a partially charge-assisted H-bond in the TS region.

Analysis of the atomic properties of the hydrogen atom involved in the CH donor group (Table 4) allows us to establish that the $C2^+H\cdots HC2^-$ DHB at the $TS_{A\cdot A^*\leftrightarrow A^*\cdot A}$ completely satisfies all eight "two-molecule" Koch and Popelier's criteria for identification of H-bonds [70]. Thus, the charge of the donor H_d hydrogen atom increases, its dipolar polarization and atomic volume decrease, the energy of the H_d hydrogen atom increases and the mutual penetration is positive (i.e., the atomic radius of the bonded atom is shorter) for both the donor H_d and acceptor H_a hydrogen atoms upon complexation. Therefore, the $C2^+H\cdots HC2^-$ DHB can be considered as a true H-bond.

Profiles of the electron density ρ, the Laplacian of the electron density Δρ, the energy E_{DHB} of the C2H···HC2 DHB estimated by the EML formula [72, 73], and the distance $d_{H\cdots H}$ between the hydrogen atoms of the C2H···HC2 DHB along the IRC of the A·A*↔A*·A tautomerization are bell-shaped with a slightly asymmetric top (in the case of the ρ, Δρ and E_{DHB} values) or bottom (in the case of the $d_{H\cdots H}$ value) (Fig. 8a, b, d, e). The electron density ρ reaches its maximum value 0.0025 a.u. at IRC=−0.53 Å and minimum value 0.0015 a.u. at IRC=−2.92 Å, while the Laplacian of the electron density Δρ reaches its maximum value 0.0093 a.u. at IRC=−0.11 Å and minimum value 0.0064 a.u. at

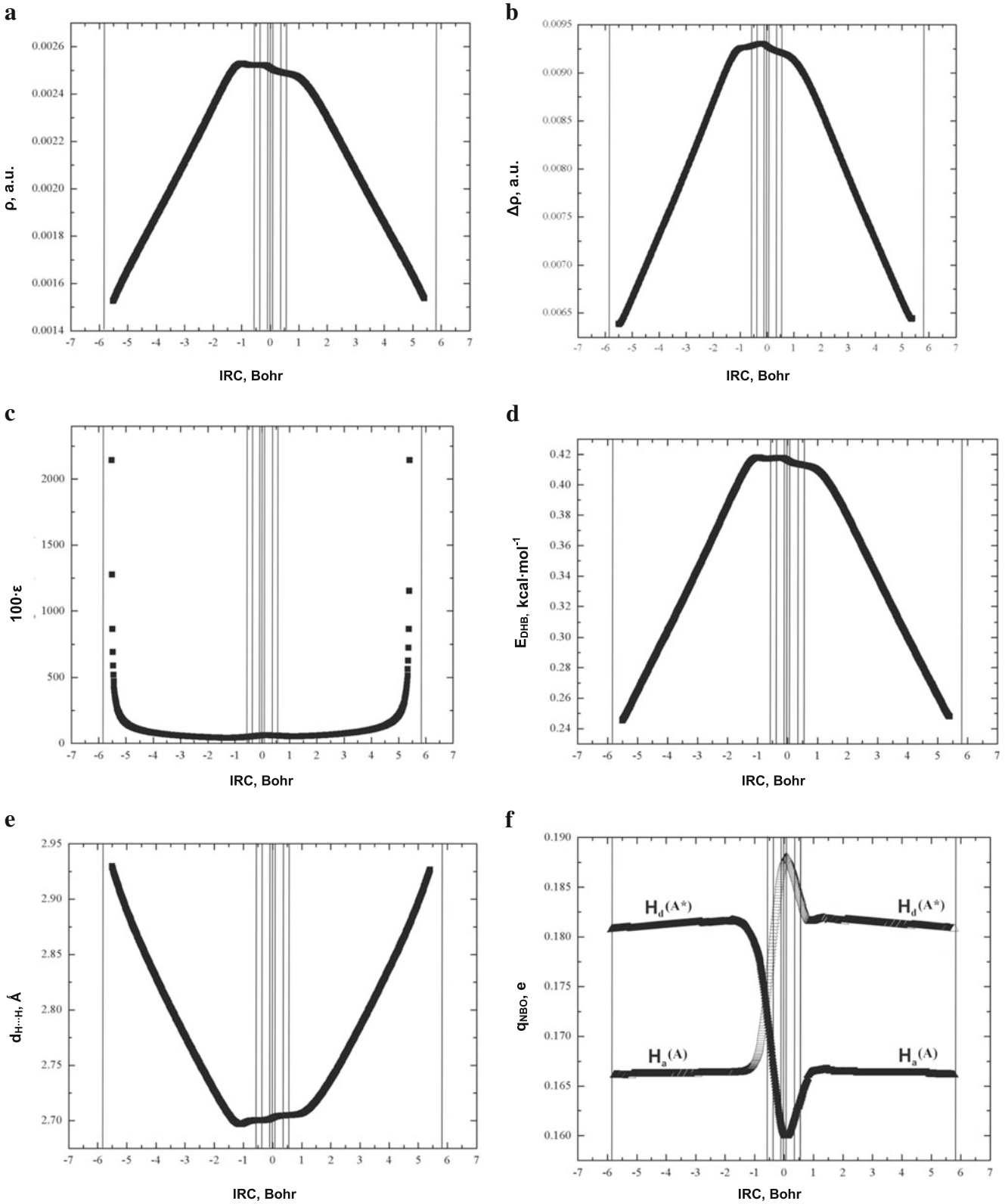

Fig. 8 Profiles of **a** the electron density ρ, **b** the Laplacian of the electron density Δρ, **c** the ellipticity ε, **d** the energy of the C2H···HC2 DHB E_{DHB}, estimated by the EML formula [72, 73], at the BCP of the C2H···HC2 DHB, **e** the distance $d_{H\cdots H}$ between the hydrogen atoms, and **f** the natural bond orbital (NBO) charges of the donor (H_d) and acceptor (H_a) hydrogen atoms involved in the C2H···HC2 DHB

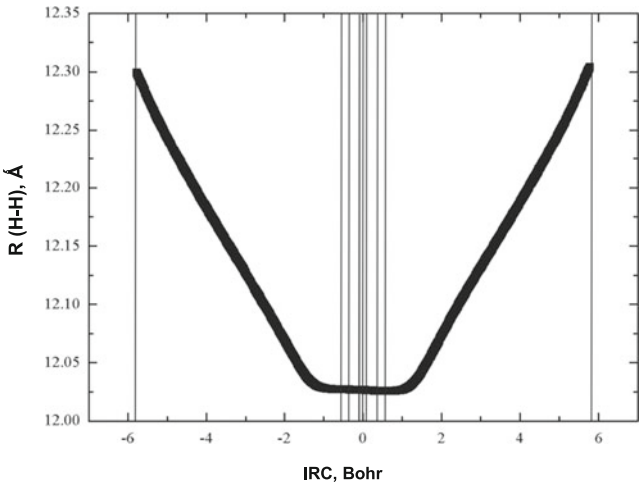

Fig. 9 Profile of the distance R(H–H) between the glycosidic protons along the IRC of the A·A*↔A*·A tautomerization via the DPT obtained at the B3LYP/6-311++G(d,p) level of theory in vacuo

IRC=−2.92 Å along the IRC of the DPT tautomerization (Fig. 8a, b). These results are within the range of values found in our recent work [93]. Extrapolation of the linear dependence $E_{HB}(\rho)$, shown in Fig. 2 in reference [88], to the value E_{HB}=0.1 kcal mol^{-1}, corresponding to the minimum value of the H-bonding energy [90], allows us to obtain the minimum value of the electron density ρ_{min}=0.0013 a.u., which almost coincides with our data ρ_{min}=0.0015 a.u. This result is in line with the results of the study reported in [88], which was devoted to the investigation of the physico-chemical properties of CH···H DHBs using ab initio QM and QTAIM methods. Profile of the ellipticity ε of the C2H···HC2 DHB is U-shaped (Fig. 8c). Ellipticity, ε, depends slightly on the IRC within the range from −2.12 to 2.12 Å and then sharply increases, varying at this within a wide range from 0.42 to 21.45 (Fig. 8c). This behavior of ε indicates that the C2H···HC2 DHB is dynamically unstable and its energy is modulated by the low-frequency intermolecular vibrations of the base pair that tautomerizes [49].

The value of Grunenberg's compliance constant [74–76] for the C2$^+$H···HC2$^-$ DHB at the $TS_{A\cdot A^*\leftrightarrow A^*\cdot A}$ is equal to 5.203 Å/mdyn, indicating that this interaction is stabilizing [53].

Electron-topological analysis shows that there is specific interaction between the donor H_d and acceptor H_a hydrogen atoms in the C2H···HC2 DHB (Tables 1, 2). NBO analysis predicts transfer of charge from σ(C2–H) bonding orbital to σ*(C2–H) anti-bonding orbital. The second order perturbation energy $E^{(2)}$, characterising the strength of this interaction, is equal to 0.19 kcal mol^{-1} at the $TS_{A\cdot A^*\leftrightarrow A^*\cdot A}$.

We have also fixed for the first time the spectroscopic manifestations of the C2H···HC2 DHB in the A·A* base pair, that tautomerizes through the DPT into the A*·A base pair. Thus, in particular, we have shown that the γ(C2H) frequency of the out-of-plane bending vibration of the C2H donor group increases by 4.5 cm^{-1} at the TS of the A·A*↔A*·A tautomerization via the DPT, which is comparable with the frequency of the corresponding vibration in the A·A* base pair, while its IR intensity increases in 3.2 times. These spectral changes are characteristic for the weak H-bonds involving CH group as the proton donor [3, 7, 22, 43, 92, 93]. These findings agree well with the elongation (0.001 Å) of the length of the CH group (A$^+$) at the $TS_{A\cdot A^*\leftrightarrow A^*\cdot A}$ (Table 1).

The lifetime of the tautomerized A*·A base pair is equal to $1.82\cdot10^{-8}$ s obtained at the MP2/cc-pVQZ//B3LYP/6-311++G(d,p) level of theory under normal conditions (Table 3). All six low-frequency intermolecular vibrations (17.4, 24.0, 61.2, 62.1, 104.2 and 105.5 cm^{-1}) are able to develop during this period of time. The time $\tau_{99.9\ \%}$ necessary to reach 99.9 % of the equilibrium concentration of the starting A·A* and the final A*·A base pair is equal to $6.29\cdot10^{-8}$ s obtained at the MP2/cc-pVQZ//B3LYP/6-311++G(d,p) level of theory under normal conditions (Table 3). This additionally indicates that the A·A* and A*·A base pairs are dynamically stable structures [43, 56, 81].

This means that the A·A* or A·A* base pair can be a source of the A* mutagenic tautomer generation at the DNA replication under the condition that it forms in the active center of the DNA polymerase. The lifetime of the A·A* or A·A* base pair exceeds by 18 times the time required for the replication machinery to forcibly dissociate a base pair into monomers (10^{-9} s [7]) during DNA replication and consequently the A·A* or A·A* base pair can dissociate successfully into A and A* monomers.

Conclusions

Combining the QM calculations and QTAIM analysis with the methodology of the sweeps of the energetic, electron-topological, geometric and polar parameters, which describe the course of the tautomerization along the IRC, we showed for the first time that biologically important planar A*·A base pair formed by the amino and imino tautomers of the adenine nucleobase tautomerizes via the asynchronous concerted DPT through the zwitterionic TS with C_s symmetry, which is the A$^+$·A$^-$ zwitterion with the separated charge, stabilized by the N6$^+$H···N6$^-$ and N1$^+$H···N1$^-$ H-bonds and the C2$^+$H···HC2$^-$ DHB. It was established that the A·A*↔A*·A tautomerization process is accompanied by significant changes in the dipole moment of the base pair (in its orientation and amplitude), i.e., this transition is dipole-active.

The nine key points for the A·A*↔A*·A tautomerization were detected and investigated thoroughly along the IRC of the tautomerization via the DPT: three key points are stationary structures, i.e., the initial state (the A·A* reactant; key point 1), the TS (key point 5) and the final state (the

A*·A product; key point 9), which is equivalent to the reactant; four key points (key points 2, 4, 6 and 8) correspond to structures where the Laplacian of the electron density equals zero at the BCPs of the N6···HN6/N6H···N6 ($\Delta\rho_{N6\cdots H}=0/\Delta\rho_{H\cdots N6}=0$) and N1···HN1/N1H···N1 ($\Delta\rho_{N1\cdots H}=0/\Delta\rho_{H\cdots N1}=0$) H-bonds, i.e., when the H-bonds become covalent bonds and vice versa; and two key points correspond to structures with the loosened N1–H–N1 (key point 3) and N6–H–N6 (key point 7) covalent bridges. Based on the sweeps of H-bond energies, it was found that two intermolecular antiparallel N6H···N6 (7.06 kcal mol^{-1}) and N1H···N1 (6.88 kcal mol^{-1}) H-bonds are significantly cooperative and mutually reinforce each other. These key points can be treated as electron-topological "fingerprints" of the asynchronous concerted tautomerization process via the DPT in any H-bonded complex whose starting geometry coincides with the final geometry.

Moreover, we established that the A·A*↔A*·A tautomerization is assisted by the third C2H···HC2 DHB in the IRC range from −2.92 to 2.92 Å. The C2H···HC2 DHB strengthens cooperatively, reaching its maximum energy 0.42 kcal mol^{-1} at the IRC=−0.52 Å and minimum energy 0.25 kcal mol^{-1} at the IRC=−2.92 Å, and is accompanied by the strengthening of the two aforementioned classical H-bonds. Here, we established that it completely satisfies the electron-topological, in particular Bader's [68] and all eight "two-molecule" Koch and Popelier's criteria [70] for H-bonding. The positive value of Grunenberg's compliance constant (5.203 Å/mdyn) proves that the $C2^{+}H\cdots HC2^{-}$ DHB at the $TS_{A\cdot A^*\rightarrow A^*\cdot A}$ is a stabilizing interaction. NBO analysis predicts charge transfer from the σ(C2–H) bonding orbital to the σ*(H–C2) anti-bonding orbital, at this point the stabilization energy $E^{(2)}$ is equal to 0.19 kcal mol^{-1} at the $TS_{A\cdot A^*\rightarrow A^*\cdot A}$.

It was shown that the A·A*/A*·A base pair is a thermodynamically ($\Delta G_{int}=-4.32$ kcal mol^{-1}) and dynamically stable structure. Its lifetime ($1.82\cdot10^{-8}$ s) exceeds by 18 times the time required for the replication machinery to forcibly dissociate a base pair into monomers (10^{-9} s [7]) during DNA replication and, consequently, the A·A* base pair dissociates successfully into A and A* monomers. This means that the A·A* base pair can be a source of A* mutagenic tautomer generation at the DNA replication on condition that it forms in the active center of the DNA polymerase.

Acknowledgments This work was partially supported by the Science and Technology Center in Ukraine (STCU) within the project № 5728 for years 2012–2014. O.O.B. was supported by a Grant of the President of Ukraine to support scientific research of young scientists for 2012 year from the State Fund for Fundamental Research of Ukraine (project № GP/F44/086) and by a Grant of the President of Ukraine for talented youth for year 2012 from the Ministry of Education and Science, Youth and Sports of Ukraine. The authors thank the Bogolyubov Institute for Theoretical Physics of the National Academy of Sciences of Ukraine for providing calculation resources and software. This work was performed using computational facilities of joint computer cluster of SSI "Institute for Single Crystals" of the National Academy of Sciences of Ukraine and Institute for Scintillation Materials of the National Academy of Sciences of Ukraine incorporated into Ukrainian National Grid.

References

1. Lehninger AL (1970) Biochemistry: the molecular basis of cell structure and function. Worth, New York
2. Rich A (1964) In: Tumerman LA (ed) Horizons in biochemistry. Mir, Moscow
3. Brovarets' OO, Hovorun DM (2013) Can tautomerization of the A T Watson-Crick base pair via double proton transfer provoke point mutations during DNA replication? A comprehensive QM and QTAIM analysis. J Biomol Struct Dynam. doi:10.1080/07391102.2012.755795
4. Hovorun DM (1997) A structural isomerism of canonical nucleotide bases: AM1 calculation. Biopolym Cell 13:127–134
5. Samijlenko SP, Krechkivska OM, Kosach DA, Hovorun DM (2004) Transitions to high tautomeric states can be induced in adenine by interactions with carboxylate and sodium ions: DFT calculation data. J Mol Struct 708:97–104
6. Danilov VI, Anisimov VM, Kurita N, Hovorun D (2005) MP2 and DFT studies of the DNA rare base pairs: the molecular mechanism of the spontaneous substitution mutations conditioned by tautomerism of bases. Chem Phys Lett 412:285–293
7. Brovarets' OO, Kolomiets' IM, Hovorun DM (2012) Elementary molecular mechanisms of the spontaneous point mutations in DNA: a novel quantum-chemical insight into the classical understanding. In: Tada T (ed) Quantum chemistry—molecules for innovations. Rijeka, In Tech Open Access, pp 59–102
8. Fonseca Guerra C, Bickelhaupt FM, Saha S, Wang F (2006) Adenine tautomers: relative stabilities, ionization energies, and mismatch with cytosine. J Phys Chem A 110:4012–4020
9. Sabio M, Topiol S, Lumma WC (1990) An investigation of tautomerism in adenine and guanine. J Phys Chem 94:1366–1372
10. Kwiatkowski JS, Leszczynski J (1992) An ab initio quantum-mechanical study of tautomerism of purine, adenine and guanine. J Mol Struct (THEOCHEM) 208:35–44
11. Salter LM, Chaban GM (2002) Theoretical study of gas phase tautomerization reactions for the ground and first excited electronic states of adenine. J Phys Chem A 106:4251–4256
12. Singh RK, Ortiz JV, Mishra MK (2010) Tautomeric forms of adenine: vertical ionization energies and Dyson orbitals. Int J Quantum Chem 110:1901–1915
13. Trakhanov SD, Yusupov MM, Agalarov SC, Garber MB, Ryazantsev SN, Tischenko SV, Shirokov VA (1987) Crystallization of 70 S ribosomes and 30 S ribosomal subunits from *Thermus thermophilus*. FEBS Lett 220:319–322
14. Wimberly BT, Brodersen DE, Clemons WM Jr, Morgan-Warren RJ, Carter AP, Vonrhein C, Hartsch T, Ramakrishnan V (2000) Structure of the 30 S ribosomal subunit. Nature 407:327–339
15. Lee JC, Gutell RR (2004) Diversity of base-pair conformations and their occurrence in rRNA structure and RNA structural motifs. J Mol Biol 344:1225–1249
16. von Böhlen K, Makowski I, Hansen HAS, Bartels H, Berkovitch-Yellin Z, Zaytzev-Bashan A, Meyer S, Paulke C, Franceschi F, Yonath A (1991) Characterization and preliminary attempts for derivatization of crystals of large ribosomal subunits from *Haloarcula marismortui* diffracting to 3 Å resolution. J Mol Biol 222:11–15
17. Kondratyuk IV, Samijlenko SP, Kolomiets' IM, Hovorun DM (2000) Prototropic molecular–zwitterionic tautomerism of xanthine and hypoxanthine. J Mol Struct 523:109–118

18. Sun X, Lee JK (2010) The stability of DNA duplexes containing hypoxanthine (inosine): gas versus solution phase and biological implications. J Org Chem 75:1848–1854
19. O'Brien PJ, Ellenberger T (2004) The *Escherichia coli* 3-methyladenine DNA glycosylase AlkA has a remarkably versatile active site. J Biol Chem 279:26876–26884
20. Hill-Perkins M, Jones MD, Karran P (1986) Sitespecific mutagenesis in vivo by single methylated or deaminated purine bases. Mutat Res 162:153–163
21. Basílio Janke EM, Riechert-Krause F, Weisz K (2011) Low-temperature NMR studies on inosine wobble base pairs. J Phys Chem B 115:8569–8574
22. Brovarets' OO, Hovorun DM (2012) Prototropic tautomerism and basic molecular principles of hypoxanthine mutagenicity: an exhaustive quantum-chemical analysis. J Biomol Struct Dynam. doi:10.1080/07391102.2012.715041
23. Brovarets' OO, Zhurakivsky RO, Hovorun DM (2013) The physicochemical "anatomy" of the tautomerization through the DPT of the biologically important pairs of hypoxanthine with DNA bases: QM and QTAIM perspectives. J Mol Model. doi:10.1007/s00894-012-1720-9
24. Frisch MJ, Trucks GW, Schlegel HB, Scuseria GE, Robb MA, Cheeseman JR, Pople JA et al (2010) GAUSSIAN 09 (Revision B.01). Gaussian, Wallingford
25. Parr RG, Yang W (1989) Density-functional theory of atoms and molecules. Oxford University Press, Oxford
26. Tirado-Rives J, Jorgensen WL (2008) Performance of B3LYP density functional methods for a large set of organic molecules. J Chem Theory Comput 4:297–306
27. Becke AD (1988) Density-functional exchange-energy approximation with correct asymptotic behaviour. Phys Rev A 38:3098–3100
28. Lee C, Yang W, Parr RG (1988) Development of the Colle-Salvetti correlation-energy formula into a functional of the electron density. Phys Rev B 37:785–789
29. Brovarets' OO, Hovorun DM (2010) How stable are the mutagenic tautomers of DNA bases? Biopolym Cell 26:72–76
30. Brovarets' OO, Hovorun DM (2010) Stability of mutagenic tautomers of uracil and its halogen derivatives: the results of quantum-mechanical investigation. Biopolym Cell 26:295–298
31. Brovarets' OO, Hovorun DM (2010) Quantum-chemical investigation of tautomerization ways of Watson-Crick DNA base pair guanine-cytosine. Ukr Biochem J 82:55–60
32. Brovarets' OO, Hovorun DM (2010) Molecular mechanisms of transitions induced by cytosine analogue: comparative quantum-chemical study. Ukr Biochem J 82:51–56
33. Brovarets' OO, Hovorun DM (2010) Quantum-chemical investigation of the elementary molecular mechanisms of pyrimidine-purine transversions. Ukr Biochem J 82:57–67
34. Brovarets' OO, Zhurakivsky RO, Hovorun DM (2010) Is there adequate ionization mechanism of the spontaneous transitions? Quantum-chemical investigation. Biopolym Cell 26:398–405
35. Brovarets' OO, Hovorun DM (2011) IR Vibrational spectra of H-bonded complexes of adenine, 2-aminopurine and 2-aminopurine^{+} with cytosine and thymine: quantum-chemical study. Opt Spectrosc 111:750–757
36. Brovarets' OO, Hovorun DM (2011) Intramolecular tautomerization and the conformational variability of some classical mutagens—cytosine derivatives: quantum chemical study. Biopolym Cell 27: 221–230
37. Frisch MJ, Head-Gordon M, Pople JA (1990) Semi-direct algorithms for the MP2 energy and gradient. Chem Phys Lett 166:281–289
38. Frisch MJ, Pople JA, Binkley JS (1984) Self-consistent molecular orbital methods 25. Supplementary functions for Gaussian basis sets. J Chem Phys 80:3265–3269
39. Hariharan PC, Pople JA (1973) The influence of polarization functions on molecular orbital hydrogenation energies. Theor Chem Accounts Theor Comput Model 28:213–222
40. Krishnan R, Binkley JS, Seeger R, Pople JA (1980) Self-consistent molecular orbital methods. XX. A basis set for correlated wave functions. J Chem Phys 72:650–654
41. Dunning Jr TH (1989) Gaussian basis sets for use in correlated molecular calculations. I. The atoms boron through neon and hydrogen. J Chem Phys 90:1007–1023
42. Kendall RA, Dunning Jr TH, Harrison RJ (1992) Electron affinities of the first-row atoms revisited. Systematic basis sets and wave functions. J Chem Phys 96:6796–6806
43. Brovarets' OO, Yurenko YP, Dubey IY, Hovorun DM (2012) Can DNA-binding proteins of replisome tautomerize nucleotide bases? Ab initio model study. J Biomol Struct Dynam 29:1101–1109
44. Pelmenschikov A, Hovorun DM, Shishkin OV, Leszczynski J (2000) A density functional theory study of vibrational coupling between ribose and base rings of nucleic acids with ribosyl guanosine as a model system. J Chem Phys 113:5986–5990
45. Shishkin OV, Pelmenschikov A, Hovorun DM, Leszczynski J (2000) Theoretical analysis of low-lying vibrational modes of free canonical 2′-deoxyribonucleosides. Chem Phys 260:317–325
46. Platonov MO, Samijlenko SP, Sudakov OO, Kondratyuk IV, Hovorun DM (2005) To what extent can methyl derivatives be regarded as stabilized tautomers of xanthine? Spectrochim Acta A Mol Biomol Spectrosc 62:112–114
47. Danilov VI, van Mourik T, Kurita N, Wakabayashi H, Tsukamoto T, Hovorun DM (2009) On the mechanism of the mutagenic action of 5-bromouracil: a DFT study of uracil and 5-bromouracil in a water cluster. J Phys Chem A 113:2233–2235
48. Yurenko YP, Zhurakivsky RO, Ghomi M, Samijlenko SP, Hovorun DM (2007) Comprehensive conformational analysis of the nucleoside analogue 2′-β-deoxy-6-azacytidine by DFT and MP2 calculations. J Phys Chem B 111:6263–6271
49. Yurenko YP, Zhurakivsky RO, Samijlenko SP, Ghomi M, Hovorun D (2007) The whole of intramolecular H-bonding in the isolated DNA nucleoside thymidine. AIM electron density topological study. Chem Phys Lett 447:140–146
50. Yurenko YP, Zhurakivsky RO, Ghomi M, Samijlenko SP, Hovorun DM (2007) How many conformers determine the thymidine low-temperature matrix infrared spectrum? DFT and MP2 quantum chemical study. J Phys Chem B 111:9655–9663
51. Yurenko YP, Zhurakivsky RO, Ghomi M, Samijlenko SP, Hovorun DM (2008) Ab initio comprehensive conformational analysis of 2′-deoxyuridine, the biologically significant DNA minor nucleoside, and reconstruction of its low-temperature matrix infrared spectrum. J Phys Chem B 112:1240–1250
52. Yurenko YP, Zhurakivsky RO, Samijlenko SP, Hovorun DM (2011) Intramolecular CH···O hydrogen bonds in the AI and BI DNA-like conformers of canonical nucleosides and their Watson-Crick pairs. Quantum chemical and AIM analysis. J Biomol Struct Dynam 29:51–65
53. Ponomareva AG, Yurenko YP, Zhurakivsky RO, van Mourik T, Hovorun DM (2012) Complete conformational space of the potential HIV-1 reverse transcriptase inhibitors d4U and d4C. A quantum chemical study. Phys Chem Chem Phys 14:6787–6795
54. Matta CF (2010) How dependent are molecular and atomic properties on the electronic structure method? Comparison of Hartree-Fock, DFT, and MP2 on a biologically relevant set of molecules. J Comput Chem 31:1297–1311
55. Lozynski M, Rusinska-Roszak D, Mack H-G (1998) Hydrogen bonding and density functional calculations: the B3LYP approach as the shortest way to MP2 results. J Phys Chem A 102:2899–2903
56. Hovorun DM, Gorb L, Leszczynski J (1999) From the nonplanarity of the amino group to the structural nonrigidity of the molecule: a post-Hartree-Fock ab initio study of 2-aminoimidazole. Int J Quantum Chem 75:245–253
57. Peng C, Schlegel HB (1993) Combining synchronous transit and quasi-Newton methods to find transition states. Isr J Chem 33:449–454

58. Peng C, Ayala PY, Schlegel HB, Frisch MJ (1996) Using redundant internal coordinates to optimize equilibrium geometries and transition states. J Comput Chem 17:49–56
59. Hratchian HP, Schlegel HB (2004) Accurate reaction paths using a Hessian based predictor-corrector integrator. J Chem Phys 120:9918–9924
60. Hratchian HP, Schlegel HB (2005) Finding minima, transition states, and following reaction pathways on ab initio potential energy surfaces. In: Dykstra CE, Frenking G, Kim KS, Scuseria G (eds) Theory and applications of computational chemistry: the first 40 years. Elsevier, Amsterdam, pp 195–249
61. Hratchian HP, Schlegel HB (2005) Using Hessian updating to increase the efficiency of a Hessian based predictor-corrector reaction path following method. J Chem Theory Comput 1:61–69
62. Boys SF, Bernardi F (1970) The calculation of small molecular interactions by the differences of separate total energies. Some procedures with reduced errors. Mol Phys 19:553–566
63. Gutowski M, Van Lenthe JH, Verbeek J, Van Duijneveldt FB, Chalasinski G (1986) The basis set superposition error in correlated electronic structure calculations. Chem Phys Lett 124:370–375
64. Sordo JA, Chin S, Sordo TL (1988) On the counterpoise correction for the basis set superposition error in large systems. Theor Chim Acta 74:101–110
65. Sordo JA (2001) On the use of the Boys–Bernardi function counterpoise procedure to correct barrier heights for basis set superposition error. J Mol Struct (THEOCHEM) 537:245–251
66. Atkins PW (1998) Physical chemistry. Oxford University Press, Oxford
67. Wigner E (1932) Über das Überschreiten von potentialschwellen bei chemischen Reaktionen [crossing of potential thresholds in chemical reactions]. Zeit Physik Chem B19:203–216
68. Bader RFW (1990) Atoms in molecules: a quantum theory. Oxford University Press, Oxford
69. Keith TA (2011) AIMAll (Version 11.12.19) Retrieved from http://aim.tkgristmill.com
70. Koch U, Popelier PLA (1995) Characterization of C-H-O hydrogen bonds on the basis of the charge density. J Phys Chem 99:9747–9754
71. Iogansen AV (1999) Direct proportionality of the hydrogen bonding energy and the intensification of the stretching ν(XH) vibration in infrared spectra. Spectrochim Acta A Mol Biomol Spectrosc 55:1585–1612
72. Espinosa E, Molins E, Lecomte C (1998) Hydrogen bond strengths revealed by topological analyses of experimentally observed electron densities. Chem Phys Lett 285:170–173
73. Mata I, Alkorta I, Espinosa E, Molins E (2011) Relationships between interaction energy, intermolecular distance and electron density properties in hydrogen bonded complexes under external electric fields. Chem Phys Lett 507:185–189
74. Brandhorst K, Grunenberg J (2010) Efficient computation of compliance matrices in redundant internal coordinates from Cartesian Hessians for nonstationary points. J Chem Phys 132:184101–184107
75. Brandhorst K, Grunenberg J (2008) How strong is it? The interpretation of force and compliance constants as bond strength descriptors. Chem Soc Rev 37:1558–1567
76. Grunenberg J, Barone G (2013) Are compliance constants ill-defined descriptors for weak interactions? RSC Adv 3:4757–4762
77. Weinhold F, Landis C (2005) Valency and bonding. A natural bond orbital donor-acceptor perspective. Cambridge University Press, Cambridge
78. Saenger W (1984) Principles of nucleic acid structure. Springer, New York
79. Govorun DN, Danchuk VD, Mishchuk YaR, Kondratyuk IV, Radomsky NF, Zheltovsky NV (1992) AM1 calculation of the nucleic acid bases structure and vibrational spectra. J Mol Struct 267:99–103
80. Nikolaienko TY, Bulavin LA, Hovorun DM (2011) How flexible are DNA constituents? The quantum-mechanical study. J Biomol Struct Dynam 29:563–575
81. Gribov LA, Mushtakova SP (1999) Quantum chemistry: textbook (Kvantovaya Khimiya: Uchebnik) (in Russian). Gardariki, Moscow, pp 317–319
82. Toro-Labbé A, Gutiérrez-Oliva S, Concha MC, Murray JS, Politzer P (2004) Analysis of two intramolecular proton transfer processes in terms of the reaction force. J Chem Phys 121:4570–4576
83. Burda JV, Toro-Labbé A, Gutiérrez-Oliva S, Murray JS, Politzer P (2007) Reaction force decomposition of activation barriers to elucidate solvent effects. J Phys Chem A 111:2455–2457
84. Jaque P, Toro-Labbé A, Politzer P, Geerlings P (2008) Reaction force constant and projected force constants of vibrational modes along the path of an intramolecular proton transfer reaction. Chem Phys Lett 456:135–140
85. Murray JS, Toro-Labbé A, Clark T, Politzer P (2009) Analysis of diatomic bond dissociation and formation in terms of the reaction force and the position-dependent reaction force constant. J Mol Model 15:701–706
86. Toro-Labbé A, Gutiérrez-Oliva S, Murray JS, Politzer P (2009) The reaction force and the transition region of a reaction. J Mol Model 15:707–710
87. Murray JS, Toro-Labbé A, Gutiérrez-Oliva S, Politzer P (2010) Identification of pseudodiatomic behavior in polyatomic bond dissociation: reaction force analysis. J Chem Phys 132:154308
88. Lipkowski P, Grabowski SJ, Robinson TL, Leszczynski J (2004) Properties of the C-H···H dihydrogen bond: an ab initio and topological analysis. J Phys Chem A 108:10865–10872
89. Grabowski SJ, Sokalski WA, Leszczynski (2005) How short can the H···H intermolecular contact be? New findings that reveal the covalent nature of extremely strong interactions. J Phys Chem A 109:4331–4341
90. Kaplan I (2006) Intermolecular interactions: physical picture, computational methods and model potentials (Wiley Series in Theoretical Chemistry). Wiley, Chichester
91. Mishchuk YaR, Potyagaylo AL, Hovorun DM (2000) Structure and dynamics of 6-azacytidine by MNDO/H quantum-chemical method. J Mol Struct 552:283–289
92. Ponomareva AG, Yurenko YP, Zhurakivsky RO, van Mourik T, Hovorun DM (2013) Structural and energetic properties of the potential HIV-1 reverse transcriptase inhibitors d4A and d4G: a comprehensive theoretical investigation. J Biomol Struct Dynam. doi:10.1080/07391102.2013.789401
93. Brovarets' OO, Yurenko YP, Hovorun DM (2013) Intermolecular CH···O/N H-bonds in the biologically important pairs of natural nucleobases: a thorough quantum-chemical study. J Biomol Struct Dynam. doi:10.1080/07391102.2013.799439
94. Bondi AJ (1964) Van der Waals volumes and radii. J Phys Chem 68:441–451
95. Gilli P, Bertolasi V, Ferretti V, Gilli G (1994) Evidence for resonance-assisted hydrogen bonding. 4. Covalent nature of the strong homonuclear hydrogen bond. Study of the O-H…O system by crystal structure correlation methods. J Am Chem Soc 116:909–915
96. Desiraju GR, Steiner T (1999) The weak hydrogen bond in structural chemistry and biology. Oxford University Press, New York
97. Lakshmi B, Samuelson AG, Jovan Jose KV, Gadre SR, Arunan E (2005) Is there a hydrogen bond radius? Evidence from microwave spectroscopy, neutron scattering and X-ray diffraction results. New J Chem 29:371–377